Research in Astronomy and Astrophysics, 24:085002 (12pp), 2024 August https://doi.org/10.1088/1674-4527/ad59ec

Investigation of WZ Sge-type Dwarf Nova ASASSN-19oc: Optical Spectroscopy and Multicolor Light Curve Analysis

Viktoriia Krushevska[1,2], Sergey Shugarov[1], Paolo Ochner[3,4], Yuliana Kuznyetsova[2], Mykola Petrov[5], and Peter Kroll[6]
[1] Astronomical Institute of the Slovak Academy of Sciences, Tatranska Lomnica, 059 60 Vysoké Tatry, Slovakia; vik.urania@gmail.com
[2] Main Astronomical Observatory of NAS of Ukraine, 27 Akademika Zabolotnoho St., 03143 Kyiv, Ukraine
[3] INAF—Osservatorio Astronomico di Padova, Vicolo dell'Osservatorio 5, I-35122 Padova, Italy
[4] Department of Physics and Astronomy, University of Padova, Via F. Marzolo 8, I-35131 Padova, Italy
[5] Max Planck Computing and Data Facility (MPCDF), Gießenbachstrasse 2, D-85748 Garching, Germany
[6] Sonneberg Observatory, Sternwartestr. 32, D-96515 Sonneberg, Germany
Received 2024 January 24; revised 2024 May 21; accepted 2024 June 11; published 2024 July 22

Abstract

In this study, we present an investigation of the newly discovered dwarf nova ASASSN-19oc during its superoutburst on 2019 June 2. We carried out detailed $UBVR_cI_c$-photometric observations and also obtained a spectrum on day 7 of the outburst, which shows the presence of hydrogen absorption lines commonly found in dwarf nova outbursts. Analysis of photometric data reveals the occurrence of early superhumps in the initial days of observations, followed by ordinary and late superhumps. We have accurately calculated the period of the ordinary superhumps as $P_{\rm ord} = 0.05681(10)$ days and determined the periods at different stages, as well as the rate of change of the superhump period ($P_{\rm dot} = \dot{P}/P = 8.1 \times 10^{-5}$). Additionally, we have derived the mass ratio of the components ($q = 0.09$), and estimated the color temperature during the outburst as ~11,000 K, the distance to the system ($d = 560$ pc) and absolute magnitude of the system in outburst ($M_V = 5.3$). We have shown that outbursts of this star are very rare: based on brightness measurements on 600 archival photographic plates, we found only one outburst that occurred in 1984. This fact, as well as the properties listed above, convincingly shows that the variable ASASSN-19oc is a dwarf nova of WZ Sge type.

Key words: (stars:) binaries (including multiple): close – (stars:) novae – cataclysmic variables – stars: dwarf novae

1. Introduction

Cataclysmic variables are close binary systems where the primary component is a white dwarf (WD) and the secondary component is a red or brown dwarf. Dwarf novae (DNe) are a class of cataclysmic variables that exhibit outburst activity. The secondary star fills its critical Roche lobe, loses mass through the inner Lagrange point L1 and accretes onto the WD. Due to the rapid orbital motion, this stream does not directly impact the WD but swirls in the direction of the orbital motion, leading to the formation of an accretion disk around the WD. Typically, the disk and its luminous structures contribute significantly to the optical radiation emitted by the system. Outbursts in DNe occur due to instabilities within the accretion disk, triggered when the gas within the disk reaches critical temperatures and densities. This temperature change results in altered viscosity, causing a portion of the matter to accrete onto the WD, releasing substantial amounts of energy. In addition to regular outbursts that last a few days, certain DNe, such as SU UMa-type stars, exhibit superoutbursts that persist for several weeks. During a superoutburst, the binary system increases its brightness by up to 6–8 mag, which is 1–2 mag higher than during a typical outburst (see, for example, Hirose & Osaki 1990; Warner 1995; Harrop-Allin & Warner 1996; Sion 1999; Hellier 2001; Osaki 2005; Giovannelli 2008; Zorotovic & Schreiber 2020).

One of the rather rare subgroups of SU UMa-type systems are WZ Sge-type stars. These stars possess the shortest orbital periods (typically 80–90 minutes) and exhibit long recurrent superoutburst intervals that can span several years or even decades, distinguishing them from other SU UMa-type stars. Notably, WZ Sge-type stars lack normal outbursts, and their superoutbursts are characterized by the largest amplitudes, reaching up to 8–9 mag (Kato 2015).

During superoutbursts of WZ Sge-type stars, a phenomenon known as "superhumps" can be observed. They are the wave-like variations in brightness with a period usually slightly longer than the orbital period. Superhumps can be classified into three categories: early, ordinary (with stages A–B–C), and late. For WZ-type stars, early superhumps are observed in the initial days following an outburst and typically exhibit a double-wave modulation with a small amplitude (up to a few hundredths of a magnitude). The period during this stage remains constant and equals the orbital period (Kato 2015; Tampo et al. 2021, 2022). However, some systems have been found to exhibit exceptionally large amplitudes of early superhumps. Our star also exhibited an early superhump

amplitude of approximately 0.1 mag, enabling us to accurately determine the period and investigate its variations. During this time, two-arm waves appear on the accretion disk, resulting in a two-peaked wave pattern on the light curves (Kato 2015). It is important to note that this phenomenon is not observed in other SU UMa-type stars.

After the early superhumps, "ordinary" superhumps appear; they usually have the maximum amplitude and the clearest variations. Whitehurst (1988), employing hydrodynamic modeling to investigate processes within accretion disks, demonstrated that such disks, in the case of a mass ratio $q = M_{\rm RD}/M_{\rm WD} < 0.25$, become tidally unstable and quickly evolve into eccentric disks. In this scenario, periodic tidal disturbances on the disk alter its brightness, leading to the appearance of superhumps (Osaki 1989, 1996, 2005; Whitehurst & King 1989; Buat-Ménard & Hameury 2002; Osaki & Meyer 2003). This model, which accounts for the simultaneous presence of both the conventional thermal instability of the disk and its tidal instability, is referred to as the "TTI model" (thermal and tidal instability).

In this model, for systems with $q < 0.25$, the disk radius can reach a value where the ratio of the orbital period of the system to the period of revolution of a physical point on the disk becomes 3:1. This resonance between the periods establishes a condition of eccentric instability, leading to increased turbulence, mass transfer rate, the onset of a superburst, and the emergence of superhumps in the light curves (Whitehurst 1988; Osaki 1989, 1996; Hirose & Osaki 1990; Kato et al. 2009a; Ringwald et al. 2012; Kato 2015; Meyer & Meyer-Hofmeister 2015). As a result, the configuration of the elliptical precessing disk, the presence of hot formations on it, and the orbital phase repeat at time intervals equal to the period of the superhumps

$$1/P_{\rm ord} = 1/P_{\rm orb} - 1/P_{\rm prec}, \quad (1)$$

where $P_{\rm ord}$ represents the period of ordinary superhumps, $P_{\rm orb}$ denotes the orbital period of the binary system, and $P_{\rm prec}$ signifies the precessional period of the elliptical accretion disk. Osaki (1989) also showed that the TTI model explains the appearance of both ordinary and superoutbursts in such types of stars.

Stage A represents the early evolution of superhumps, during which their amplitude increases, and a consistent period is observed, which is longer than that in Stage B. During stage B, superhumps are most prominently observed, and their period can be determined with high accuracy. Throughout this stage, the period length exhibits a nearly linear time variation. This variation is quantified by the value $P_{\rm dot} = \dot{P}/P$, which represents the rate of period change relative to the period itself. Kato et al. (2009a, 2016a, 2016b, 2017) extensively studied this value for nearly a thousand SU UMa- and WZ Sge-type stars. For systems with a short orbital period, $P_{\rm dot}$ is typically positive. From Equation (1), it is evident that the observed superhump period is the beat period between the orbital period and the precessional period of the accretion elliptical disk. The size of the disk, and consequently the precessional period, slowly changes after the outburst, leading to a variation in the superhump period. (For more details on the physics of this phenomenon, see, for example, Hirose & Osaki (1990), Lubow (1991), Kato et al. (1998), Uemura et al. (2005), Soejima et al. (2009).) In the final stage C, superhumps become less distinct, with a usual decrease in amplitude and a shorter period compared to stage B. Hence, the superhump period, amplitude, color indices, and the stability of the light curve variate at each stage (Kato et al. 2009a, 2017). By this time, the star's brightness decreases by several magnitudes. The stages A–B–C and the transitions between them are shown in great detail in the work of Kato (2022a).

In most cases, the period of superhumps is a few percent longer than the orbital period, as indicated by Equation (1), and these brightness variations are referred to as "positive superhumps." However, if the period of the superhumps is slightly shorter than the orbital period, they are termed "negative" superhumps. The presence of "negative" superhumps can be attributed to the inclination of the accretion disk relative to the orbital plane and its simultaneous nutation motion. Further explanations of this phenomenon can be found in Udalski (1988), Harvey et al. (1995), Wood & Burke (2007), Wood et al. (2009), Ohshima et al. (2014), and Thomas & Wood (2015). Note that to explain the behavior of stars with superoutbursts, there are models alternative to TTI, for example, "the enhanced mass transfer" model (Hameury et al. 2000; Lasota 2023). There are also theories that partially combine both models: (e.g., Smak 2000, 2009, 2020). A comparison of different models explaining processes in WZ Sge stars can be found, for example, in Lasota (2001).

Some WZ Sge-type stars may exhibit recurrent increases in brightness at the end of a superoutburst, known as rebrightenings or "echo outbursts." These rebrightenings are shorter in duration, with a smaller amplitude increase in brightness up to 2–3 mag. Based on the light curve shape, rebrightenings can be classified as long-duration, multiple, or single events (Imada et al. 2006). For example, EZ Lyn showed 11 rebrightenings (Kato et al. 2009b), ASASSN-15po had 10 rebrightenings (Kato 2015; Namekata et al. 2017), EG Cnc exhibited 6 rebrightenings (Kimura et al. 2021), and MASTER OT J211258.65+242145.4 displayed 8 rebrightenings (Nakata et al. 2013), among others. The occurrence of rebrightenings can be associated with the behavior of the accretion disk. During an outburst, the accretion disk heats up significantly and increases in size. In this situation, the inner part of the disk becomes optically thick, obscuring the light from the WD, causing the apparent brightness of the star to decrease. However, as the outburst progresses, the disk begins to cool and thin out, leading to an increase in the light flux from the WD once again. The phase of rebrightening can be

quite substantial and may sometimes exceed the initial peak brightness of the outburst. A potential explanation for this phenomenon is provided by Meyer & Meyer-Hofmeister (2015).

The goal of this study was to obtain multicolor photometry of the object ASASSN-19oc, to conduct a detailed analysis of superhumps and, based on the system parameters, to verify its classification as a WZ Sge-type system.

2. Observations

The object ASASSN-19oc (AT 2019gvn, $\alpha 2000 =$ 19:49:06.773, $\delta 2000 = +10{:}06{:}58.27$)[7] was discovered on 2019 June 2 (JD 2458636.70) by the All-Sky Automated Survey for Supernovae (ASASSN, see Shappee et al. 2014), as described in vsnet-alert 23282[8] and, based on the large outburst amplitude, was identified as a candidate for cataclysmic variables of the WZ Sge-type. This outburst was independently discovered by the Brazilian Transient Search (BraTS) team (JD 2458636.74) and reported to the Transient Name Server (TNS) (report № 36916, Jacques et al. 2019). Three days later, on June 5, early superhumps were identified, characterized by a preliminary period of 0.0546(5) day and an amplitude of 0.09 mag (vsnet-alert 23291). On June 7, Josch Hambsch and Tonny Vanmunster (vsnet-alert 23293) refined the early period of the superhumps to 0.05564(4) days and indicated the presence of double-hump modulation. On June 11, Josch Hambsch announced the beginning of the ordinary superhump phase (vsnet-alert 23309).

2.1. Photometric Observations

We have conducted photometric observations of ASASSN-19oc using the $UBVR_CI_C$- passbands at the 50 cm (AZT-5) and 60 cm (Zeiss-600) telescopes located at the South station of SAI, using Apogee Alta U16M and Apogee Aspen CG-42 CCD cameras, respectively. The observations spanned from 2019 June 3 to 18 and we obtained about 300 images. On different nights, the exposure varied from 30 to 105 s, depending on weather conditions and brightness of the variable. The MaxIM DL4+DSLR program was used for the frames processing. Standard procedures of bias, dark-frame subtraction and flat field correction were performed. For data reduction we have selected six comparison stars in the field of ASASSN-19oc as marked in the left panel of Figure 1. The magnitudes of these comparison stars were tied to standards in the SA112 region of Landolt's fields (Landolt 2009) which we observed in 2021 October in the Astronomical Institute of SAS using the Zeiss-600 telescope and the FLI ML3041 CCD camera. The values of their magnitudes calculated by us are presented in Table 1. Based on this, we calculated the nightly mean magnitudes of ASASSN-19oc for each U, B, V, R_C and I_C band and indicated them in Table 2. The number of frames per night and the used telescopes are also listed.

We also processed about 600 archival photographic negatives stored at the Sonneberg Observatory for the period 1932–1995. Observations were carried out on telescopes GA, GC (400/1600), GB (40/2000), "A camera" (170/1200) and "Schmidt camera" (500/700/1720). All photographic plates were initially examined visually by the microscope. The star was visible on only six negatives obtained in 1984 July with a GC-astrograph, (Figure 1, right), probably at the plateau stage after the nonregistered maximum. These six photographic plates were scanned, and then the magnitude of the variable star was measured relative to the stars in Table 1. The processing results are presented in Table 3. In all cases unsensitized photographic plates were used, so the photosensitivity of the photographic emulsion with the glass objective that blocked UV-rays (except "Schmidt camera") was within the range of about ~4000–5000 Å. This range is close to the B band of the Johnson system. Therefore, we calibrated the negatives using the B-magnitudes from Table 1 (see Table 3, as well as Figure 4).

2.2. Spectral Observations

Spectral observations were obtained on 2019 June 9 at Asiago Astrophysical Observatory using the 1.22 m Galileo Galilei Telescope fitted with the B&C spectrograph (resolution 6 Å and range 3300–7500 Å).[9] One spectrum of ASASSN-19oc was obtained with an exposure time of 1800 s. The spectrum of ASASSN-19oc is presented in Figure 2 along with the spectrum of the standard star HR 5501 for better visual identification of the detected spectral lines. Other spectral data for this object can be seen on the Transient Name Server (the spectrum shown there is similar to ours)[10] (Frohmaier et al. 2019).

The spectrum of the transient shows a blue continuum with broad Balmer absorption lines. We estimated the full width at half maximum (FWHM) and equivalent width (EWs) for detected spectral lines for whole line and for core of line (central portion of line without wings) separately and expressed them in Table 4. For this, the spectrum was normalized by dividing by the fitted continuum. The very weak H_α λ 6563 line is almost invisible. $H_\beta - H_\delta$ are clearly visible, and H_ε is better detected after removal of continuum.

Such a spectrum, in which high-order Balmer absorption dominates during an initial outburst stage, is typical for DNe (Hessman et al. 1984). In particular, it was also observed in other SU UMa-type stars, for example, in V521 Peg, QW Ser (Szegedi et al. 2017), V344 Lyr, RZ LMi (Han et al. 2020), and PNV J00215475+5231007 (Taguchi 2023). The spectra of 11

[7] Gaia Early Data Release 3 (Gaia EDR3) (see Gaia Collaboration et al. 2021).

[8] All alerts are available via http://ooruri.kusastro.kyoto-u.ac.jp/mailarchive/vsnet-alert/2019-June/thread.html.

[9] Technical data are noted here: http://www.astro.unipd.it/inglese/observatory/obs_en.htm.

[10] https://www.wis-tns.org/object/2019gvn (orange graph).

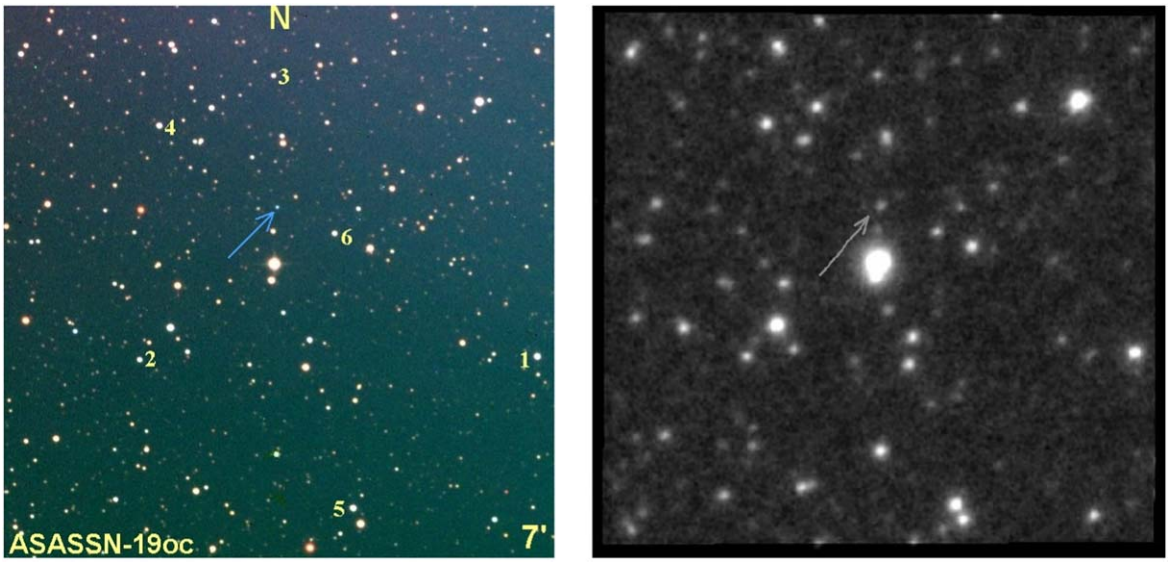

Figure 1. Color map of the ASASSN-19oc field constructed using a combination of frames obtained in the B, V, and I_C bands (left); a scan of the photographic plate with the outburst in 1984 (right).

Table 1
Comparison Star Magnitudes

Number	U	B	V	R_C	I_C	$B-V$
1	14.30	14.21	13.52	13.06	12.70	0.69
2	15.61	15.30	14.53	14.05	13.71	0.77
3	16.08	15.95	15.08	14.51	14.05	0.87
4	15.07	14.85	14.02	13.51	13.12	0.83
5	14.75	14.37	13.58	13.08	12.72	0.79
6	15.87	15.54	14.52	13.89	13.38	1.02

Note. The accuracy of values for U is 0.05–0.1 mag, that for B and V is 0.02–0.03 mag, and that for R_C and I_C is 0.01–0.02 mag.

DNe during outbursts (AR And, X Leo, CZ Ori, etc.) are also considered in the article of Szkody et al. (1990). These stars also have absorption lines, and their nature is considered by the authors of this paper. The absorption in the Balmer lines points out that the accretion disks in these systems are optically thick during the outbursts.

Modeling spectra based on theoretical calculations at certain stages of the outburst also indicates the presence of absorption lines under the corresponding conditions of matter in the disk (see, for example, Kromer et al. 2007; Idan et al. 2010; Hubeny & Long 2021).

3. Data Analysis

3.1. Light Curves and Color Variations

Analysis of our photometric observations of the ASASSN-19oc superoutburst showed early, ordinary, and late superhumps. In Figure 3, at the bottom, we indicated these stages with arrows. The criterion for their distinction was the presence of a double wave per period (early superhumps), maximum amplitude and clear brightness oscillations (ordinary superhumps), as well as less distinctly expressed brightness variations with a period close to that of ordinary superhumps (stage C of ordinary superhumps progressing to late ones). Here, we present the brightness decline curve of ASASSN-19oc during this superoutburst. The red circles represent our data in the R_C-passband, while the asterisks indicate observational data from American Association of Variable Star Observers (AAVSO) (without filters). In the inner insets we can see the double waved oscillations corresponding to early superhumps and very clear ordinary superhumps at stage B.

At stage C, a wave with a period close to that of ordinary superhumps is identified only when processing all data using the Fourier method (see Figures 5 and 6(c)). However, on certain nights, the periodicity was very weakly expressed or completely absent (see inset "c" in Figure 3). In Section 3.2, we will provide the proposed temporal boundaries for the intervals of these stages. More detailed descriptions of these stages for WZ Sge-type system stars are given in Kato (2015). No rebrightenings (repeated short-term brightenings after a superoutburst) were detected for this system.

To estimate the magnitude of this object before the superoutburst, we processed all its available images from the PanSTARRS-1 survey, as well as our observations obtained in 2021 October, when the star was at quiescence. Analysis of the data showed that the object was 20.8 mag in the red passband r ($\lambda_{\rm mean} = 6215$ Å) and 21.8 mag in the blue passband g ($\lambda_{\rm mean} = 4866$ Å). Similar brightness estimates were obtained

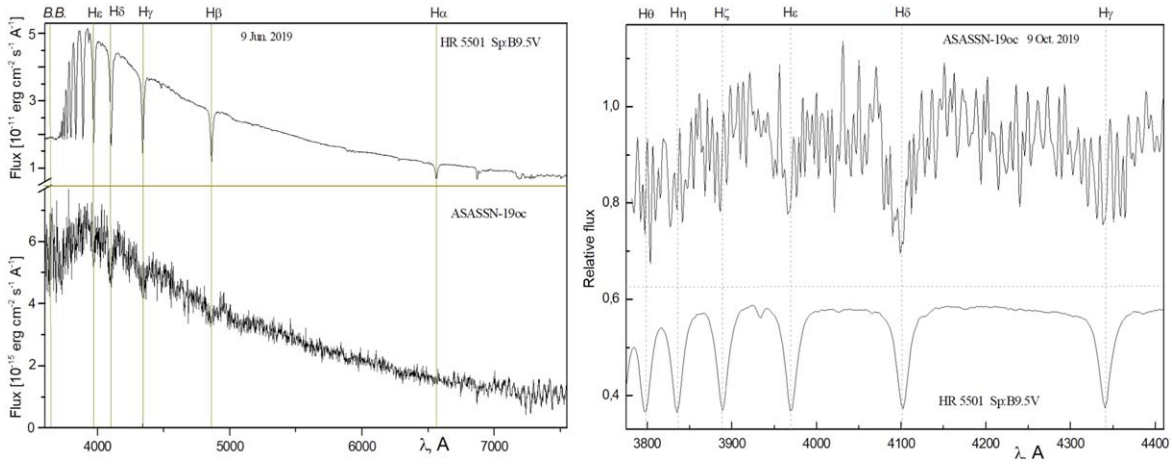

Figure 2. Spectra of ASASSN-19oc and standard star HR 5501 obtained on 2019 June 9 in Asiago Observatory with the 1.22 m Galileo Galilei Telescope (Italy). Hydrogen lines and Balmer break (BB) are marked. Left panel: spectra in wide diapason; Right panel: normalized spectra in the region of high-order Balmer lines in spectral range 3800–4400 Å.

Table 2
Log of Observations

JD	U	N_U	B	N_B	V	N_V	R_C	N_{R_C}	I_C	N_{I_C}	Tel.
2458638.52	13.86	1	14.37	21	14.44	23	14.25	29	14.27	22	AZT-5
2458640.48	14.34	1	14.85	29	14.87	32	14.67	66	14.68	32	AZT-5
2458643.54	⋯	⋯	15.28	2	15.37	3	15.17	3	15.10	2	AZT-5
2458644.53	⋯	⋯	15.49	6	15.48	10	15.25	15	15.19	4	AZT-5
2458647.49	15.58::	1	15.83	11	15.83	14	15.54	53	15.57	10	AZT-5
2458648.44	15.48::	1	16.00	11	15.96	13	15.70	46	15.70	9	AZT-5
2458649.54	15.66::	1	15.98:	2	16.13:	2	15.86:	5	15.94	2	AZT-5
2458650.53	⋯	⋯	16.21	3	16.20	8	15.98	16	15.91:	6	AZT-5
2458651.53	⋯	⋯	16.55:	2	16.35	3	16.07	8	15.97:	2	Zeiss-600
2458652.45	⋯	⋯	⋯	⋯	⋯	⋯	16.22	25	⋯	⋯	Zeiss-600

Note. The measurement accuracy for unmarked magnitudes is ±0.01–0.03 (*BVRI*) and 0.07–0.10 (*U*). Values marked with the symbol ":" have an accuracy of up to ±0.05 – 0.10, and those with the symbol "::" up to ±0.12 – 0.15 mag.

Table 3
B_{pg}-magnitudes of ASASSN-19oc During the 1984 Outburst

JD	2445905.43	2445905.49	2445909.44	2445911.47	2445911.48	2445913.51
B_{pg}	15.93	15.89	16.34	16.35	16.65	⩾17.3

Table 4
Equivalent Widths of the most Significant Spectral Lines of ASASSN-19oc

Line	FWHM, Å Line	EW, Å Line	FWHM, Å Core of Line	EW, Å Core of Line
H_β (4861,3)	30	5	19	3.5
H_γ (4340,5)	35	5.6	8	1.9
H_δ (4101,8)	39	7.7	20	4.8
H_ε (3970,1)	22	3	8	1.6

on our CCD frames. Therefore, we can conclude that the superoutburst amplitude is about 7 mag.

Figure 4 (bottom panel) depicts our nightly average R_C observations, AAVSO observations (*CV*) shifted to R_C by −0.3 mag, and our *B*-band observations (blue open circles) for the year 2019. Photographic measurements B_{pg} during the 1984 outburst (blue snowflakes) are also plotted on this graph. When plotting these old data, the timescale was shifted so that the deviation (in magnitude) of the archival observations of 1984

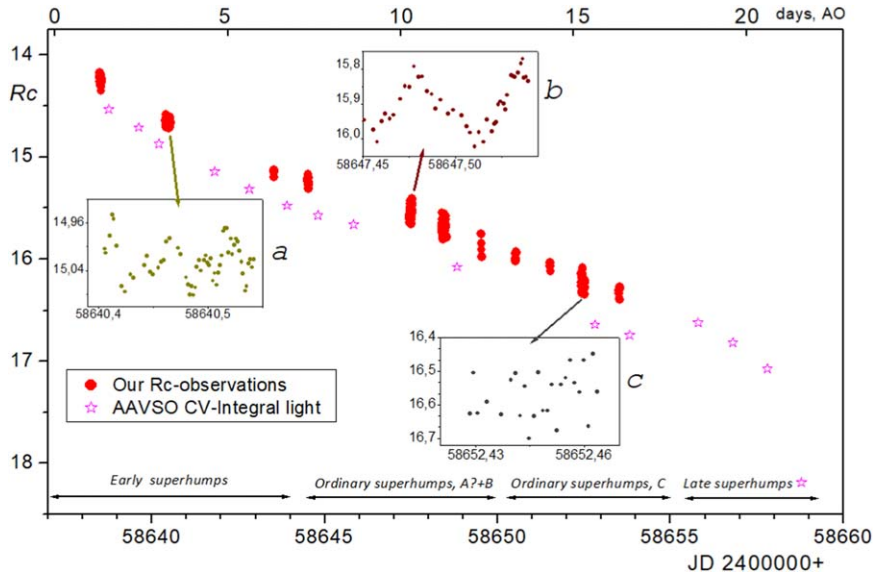

Figure 3. The decline of brightness of ASASSN-19oc. The insets show brightness variations during several nights at the different stages of superhumps. At the top is the number of days after the outburst maximum (AO). Approximate intervals of the various superhump stages are also displayed.

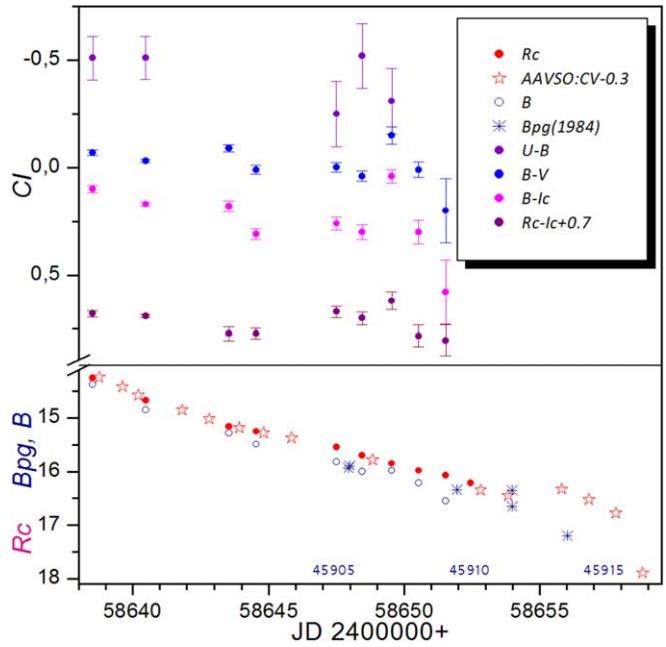

Figure 4. Color-indices (upper) and brightness (lower) variations of ASASSN-19oc during the superoutburst (taken from Tables 2 and 3). The light curve is composed by our R_C- and B-passband data (red and blue circles, respectively), AAVSO data (red asterisks), and B_{pg} data from 1984 (blue snowflakes).

from the new ones of 2019 was minimal. The 1984 timeline is labeled in blue above the 2019 timeline. We see that the 1984 observations fell at the middle of the plateau stage of the outburst. Moreover, we can conclude that the interval between outbursts may be about 35 yr. Since the duration of the outburst together with the plateau is about 20 days (see Figures 3 and 4), some past outbursts could certainly have been missed due to the irregular time coverage of archival observations and the invisibility of ASASSN-19oc (constellation Aquila) at the Sonneberg Observatory (Germany) during the winter season. Therefore, the average interval between outbursts may be shorter than 35 yr. However, the fact that out of 600 archival measurements the object was visible in only 6 allows us to conclude that outbursts from the ASASSN-19oc occur rarely, which is typical for stars of the WZ Sge type.

To analyze changes in color indices over time, we calculated the following values $R_C - I_C$, $B - I_C$, $B - V$ and $U - B$, and presented them in the top panel of Figure 4. Their variations point to a slight increase in the values of all indices over time, i.e., to the redness. (Note that the changes in the $R_C - I_C$ color index are within the measurement errors.) This behavior is typical for DNe (Lee et al. 2019).

3.2. Periods of Superhumps at Different Stages

To study the short-period waves (superhumps), it was necessary to remove the trend caused by the fading of the variable's brightness after the outburst. Detrending was performed using the "piecewise quadratic splines" method with our custom code, which was slightly modified to account for the observed brightness decline of the studied star. For this, we fitted smoothed curves using all data for the $UBVR_CI_C$ bands as well as data taken from AAVSO (CV band). Subsequently, we calculated the differences (deviations)

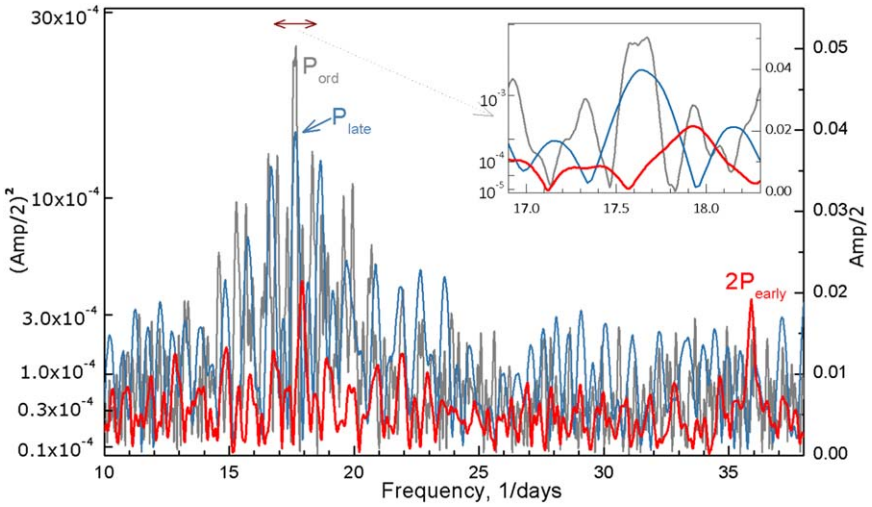

Figure 5. Fourier-spectrum calculated for early (red line), ordinary (gray line) and late (blue line) superhumps (SH). The *Y*-axes show the square of half-amplitude (left) and half-amplitude (right) of the periodic wave for the respective superhumps. Note that the early superhump period is shorter than that of ordinary superhumps.

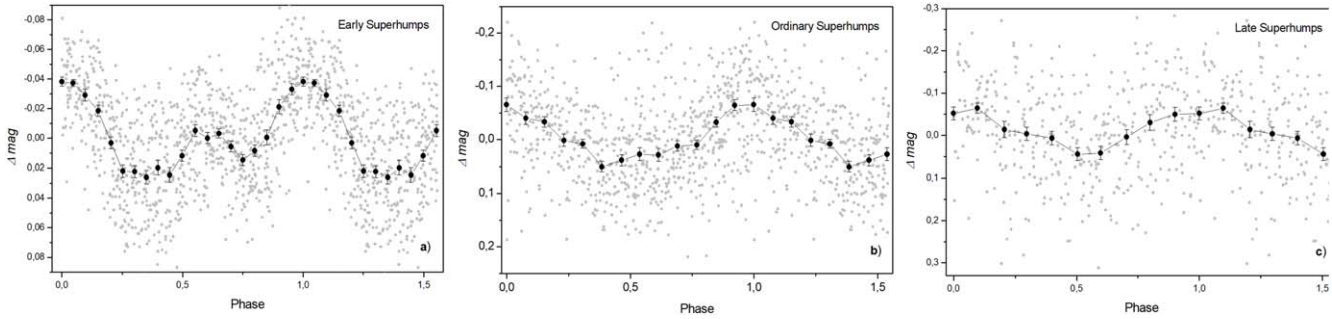

Figure 6. Light curves during superoutburst, phase-folded with the early (a), ordinary (b) and late (c) superhump period (our and AAVSO data). There is a double wave for early superhumps and a single wave for ordinary and late superhumps per period.

between the original data and these curves. These detrended values were then utilized for periodogram analysis.

As these differences oscillated around zero for all photometric bands, for more accurate period calculation, in some cases we combined them into one common summary file for improved statistics. We also conducted a similar procedure to study the color variations in the system's brightness separately in each band.

To analyze the periodicities over limited time intervals corresponding to different stages of superhumps, we used our own code based on the Discrete Fourier Transform method (similar to the code from Deeming 1975). The shape of the superhumps is close to sinusoidal, so this approximation is acceptable. The resulting periodogram is presented in Figure 5.

Between JD 2458638 and JD 2458644, the system exhibited early superhumps, which can appear in WZ Sge-type stars during the initial days following the start of a superoutburst and which represent a double wave over a period (see "Introduction"). The period we found at this stage is $P_{\rm ear} = 0.055685$ days. The data phase-folded with this period are plotted in Figure 6(a). The period of early superhumps closely aligns with the orbital period, as also mentioned in the "Introduction." On average, the early superhumps exhibited an amplitude of 0.06 mag, although on certain nights, it reached 0.09 mag, as depicted by the inner curve labeled as "Early SH" in Figure 3.

Beginning from JD 2458644 and until JD 2458650, ordinary superhumps appear in the system (stages A and B, see inner curve "Ordinary SH, stage B" in Figure 3).

From JD 2458650, stage C of ordinary superhumps begins, passing into late superhumps (JD 2458655–2458658). Significant variability can be observed in the light curves obtained on specific nights, as indicated by the inner curve labeled as "Ordinary SH (stage C)" in Figure 3.

During stages A–B, we determined the average period of superhumps to be $P_{AB} = 0.05674(10)$ days. It can be assumed

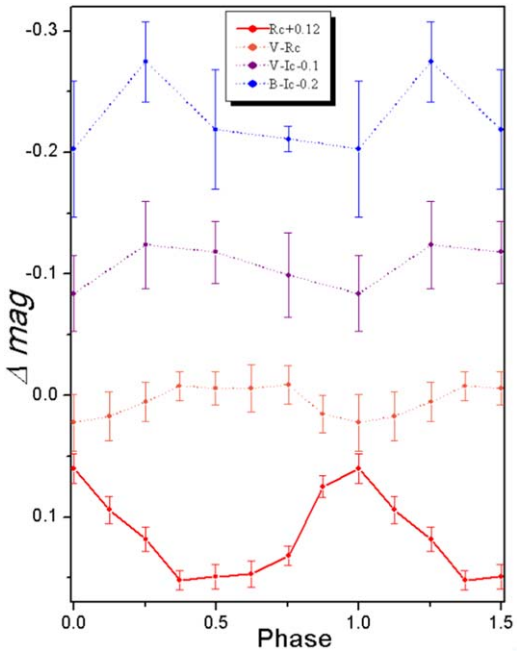

Figure 7. Color indices phase-folded with P_{ord}. The lower curve represents the phase curve built for ordinary superhumps (stages A–B), while the upper curves are the change in color indices with the superhump phase. It can be seen that during the superhump maximum, $V-R$ color indices increase, i.e., the star becomes redder. The changes in $B-V$ and $R-I$ color indices with phase probably have a similar form but are within the data dispersion on the phase curve.

that stage A, during which the superhump period undergoes minimal changes, was either very short or skipped. Therefore, all the described facts can be realistically attributed to stage B. The average amplitude was 0.20 mag, reaching a value of 0.25 mag on some nights. During stage C (JD 2458650–2458655), the average superhump period was $P_C = 0.0570(4)$ days, and the average superhump amplitude decreased to 0.07 mag. Convolution with this period shows a large dispersion.

The average period of superhumps determined by Fourier method for all three stages (A–B–C) was found to be $P_{ord} = 0.05681(10)$ days (Figure 6(b)).

For late superhumps, we found a period close to that of stage C, but due to the highly unstable light curve, the period error is big: $P_{late} = 0.057(3)$ days (Figure 6(c)).

As we wrote in the "Introduction," the superhump period is not permanent. Below we describe these changes in more detail.

In Figure 7, we display the color index variations depending on the phase of ordinary superhump period. We can see that $V-R$ and $V-I$ color indices are bluest at phases around 0.5, i.e., during the superhump minimum. Very similar color changes for other DNe were found by Neustroev et al. (2017), Lee et al. (2019).

To clarify the nature of the change in the period at the stage of ordinary superhumps, the deviations of the period from the value of $P_{ord} = 0.056812$ days were calculated. From our and AAVSO data, we built the corresponding $O-C$ diagram, taking $E_0 = 2458648.4425$ as the initial epoch (Figure 8). Both times of maxima and times of minima were taken into account. From this figure, it is evident that during early superhumps, their period remained constant (a straight line on the graph) and was equal to $P_{ear} = 0.055685$ day. The average period of ordinary superhumps ($P_{ord} = 0.05674$) was greater than the period of early superhumps. In Figure 8, it can also be observed that during this time, the $O-C$ values have a parabolic shape. This indicates that the observed period linearly increased with time. By finding the coefficients for this parabolic approximation, we determined the rate of period change $P_{dot} = \dot{P}/P = 8.1 \times 10^{-5}$.

Such period changes are observed in most SU UMa- and WZ Sge-type stars and are described in detail in a series of papers by Kato (see Kato et al. 2009a, 2017; Kato 2015). The period of late superhumps may again be constant (Kato et al. 2009a), but our observations, due to their small number, do not allow us to confidently detect it at this stage. In the article by Kato (2022a), the outburst of the star V844 Her (WZ Sge-type) was described in great detail; using the TESS data, the author studied and analyzed this entire series of observations within 20 days after the outburst with a time resolution of several minutes. In the cited work, the light curve is confidently traced in stages A–B–C and, probably, at the beginning of the late superhumps. Transitions between these stages are also noticeable. The orbital periods of ASASSN-19oc and V844 Her are close (0.0556 and 0.0546 day respectively). It will be shown below that the mass ratios q for these stars are also close ($q = 0.09$ for ASASSN-19oc and $q = 0.084$ for V844 Her (Figure 3 in Kato 2022a)).

3.3. Two-color Diagrams and Determination of System Parameters of ASASSN-19oc

Figure 9(a)–(c) shows the positions of ASASSN-19oc with the number of days that have passed since the outburst, and the comparison stars on three different two-color diagrams. To plot the unreddened positions of neighboring stars and the displacements of the variable on two-color diagrams, it is necessary to know the value of the interstellar reddening $E(B-V)$. $E(B-V)$ is the object's reddening which is equal to the difference between the object's observed color index $(B-V)$ and its true color index $(B-V)_0$, so that $E(B-V) = (B-V) - (B-V)_0$.

On the $U-B/B-V$ diagram (Figure 9(a)), we can estimate this value from the deviation of the position of the field of neighboring stars, which most likely belong to either main sequence stars or giants. On the indicated diagram we shift the positions of these stars parallel to the interstellar reddening line by ~0.25 mag.

Note that this method is only an estimate; among neighboring stars there may be distant bright giants that have a larger

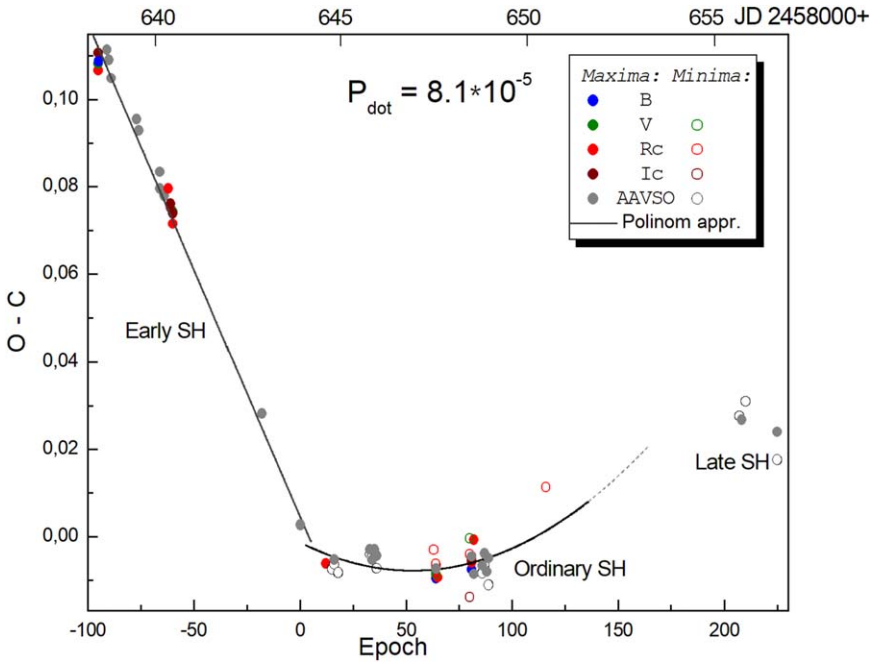

Figure 8. $O-C$ diagram showing the variation in superhump periods in the ASASSN-19oc superoutburst with used $P_{\rm ord} = 0.056812$ day and $\rm JD_0 = 2458648.4425$.

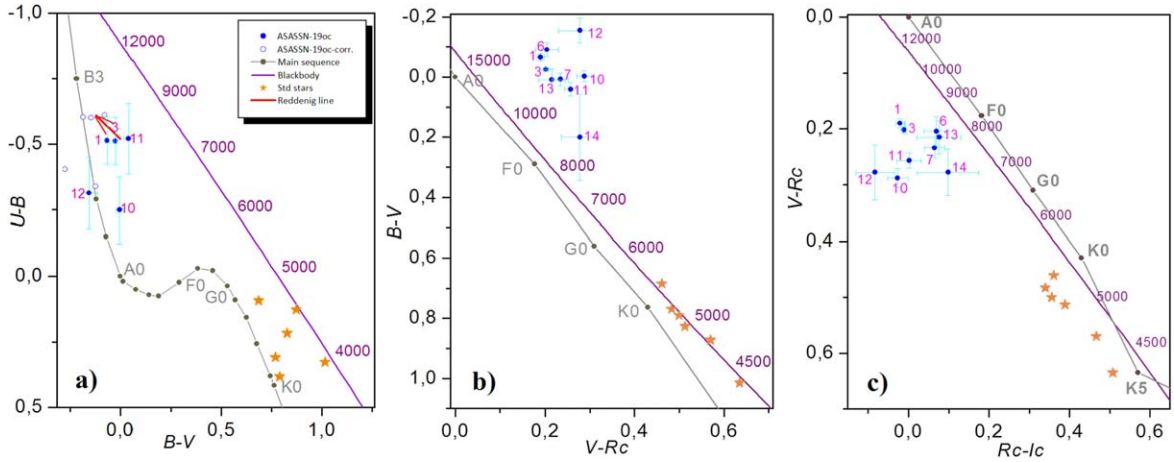

Figure 9. Two-color diagrams of ASASSN-19oc. Main sequence and blackbody line are plotted with gray and purple, respectively. The blue dots (with cyan errors) mark the position of ASASSN-19oc. The numbers around these dots indicate the number of days since the maximum of superoutburst (as described in Figure 3). Blue open circles show the same positions of the variable, but shifted with average interstellar reddening $E(B-V) \sim 0.12$ mag (see text). The positions of neighboring field stars are indicated by orange asterisks.

extinction $E(B-V)$ than closer stars and the variable itself, therefore we consider the resulting reddening value of 0.25 mag to be an upper limit: $E(B-V) < 0.25$ mag.

To more accurately determine the value of $E(B-V)$, it is necessary to know the distance to the system. We can calculate it using the standard formula

$$d = 10^{0.2(V-M_V+5-A_V)}, \quad (2)$$

where A_V is the extinction in the V band.

At the maximum of the superoutburst the visible magnitude of ASASSN-19oc was $V \sim 14.4$ mag (see Table 2). According to Kato (2015), the absolute magnitude during the maximum of a superoutburst of SU UMa-type stars is $M_V\,(\rm max) = 5.64–0.259 \times P_{\rm orb}\,(\rm hr)$. For $P_{\rm orb}$ of most stars of the WZ Sge-type and our object this formula gives $M_V\,(\rm max) = 5.3$. So, $V - M_V = 9.1$. The value of interstellar extinction $A_V = 3.1E(B-V)$. Therefore if $0 < E$

$(B-V) < 0.25$ then $0 < A_V < 0.8$. According to formula (2), if A_V is close to zero, we obtain a distance to the system of 660 pc, and if $A_V = 0.8$ the distance is 470 pc.

Using modern three-dimensional (3D) dust maps that trace reddening as a function of both the object's angular position in the sky and its distance, we can more accurately estimate $E(B-V)$ values. For the boundary distances of 470 and 660 pc, we will find the corresponding values of $E(B-V)$ from the following 3D maps:

1. "A 3D Dust Map Based on Pan-STARRS 1, Gaia and 2MASS"[11] (Green et al. 2019) gives us values from 0.12 to 0.16;
2. from "STructuring by Inversion the Local InterStellar Medium" (Stilism)[12] (Lallement et al. 2014; Capitanio et al. 2017) we get values from 0.09 to 0.11;
3. "Gaia-2MASS 3D maps of Galactic interstellar dust extinction within 3 kpc"[13] (Lallement et al. 2019) gives values from 0.11 to 0.12.

The average value of $E(B-V)$ by these three sources is 0.12 ± 0.03 and then A_V will be equal to 0.37 ± 0.1. As a result, using formula (2), we obtain the distance to the system of $d = 560 \pm 50$ pc.

The diagram in Figure 9(a) also includes a red arrow corresponding to interstellar reddening by $E(B-V) = 0.12$ mag, as well as field stars, main sequence, and the blackbody line. It can be seen that ASASSN-19oc has a significant excess of $U-B$ (Figure 9(a)) and $B-V$ (Figure 9(b)) values—the object is located above the main sequence line. This is because the hot accretion disk gives a large contribution to the overall flux from the system. The maximum radiation from the disk (according to Planck's law) is in the UV region of the spectrum, which is also evident from the energy distribution curve in the spectrum in Figure 2. We see that the outburst color temperature, corrected for interstellar reddening, can be estimated as ~10,000–11,000 K and at the end of our observational set, it decreased by about 3000 K. Note that the average color temperature in the $V-R/R-I$ diagram is lower than in the other two diagrams. This is due to the fact that in the red and near-infrared wavelengths, the main radiation comes from the colder parts of the accretion disk and the red dwarf, and therefore the average color temperature (taking into account interstellar reddening) is lower and varies from ~10,000 K during the outburst up to ~8000 K by the end of our observations.

Similar behavior is typical for the majority of cataclysmic binaries including WZ Sge-type stars. During the superoutburst DNe move along and below the blackbody line (Bruch 1984; Echevarría 1984). Numerical simulations carried out by Mayo et al. (1980) and Echevarría & Jones (1983) attribute this behavior to the variability in the luminosity of the accretion disk. A detailed study of DNe tracks on a color–color diagram was shown also by Bailey (1980) and Cannizzo & Kenyon (1987).

Knowing both the orbital period and the period of the superhumps, it becomes possible to calculate the superhump excess, the value ε: $\varepsilon = (P_{\rm ord}/P_{\rm orb}) - 1$. For WZ Sge-type stars, orbital period $P_{\rm orb}$ is approximately equal to period of early superhumps $P_{\rm ear}$ (Kato 2015), so $\varepsilon = (0.056812/0.055685) - 1 = 0.020$. This value is commonly observed for SU UMa-type stars, including the subgroup of WZ Sge-type stars (see the distribution of ε for SU UMa stars in Kato et al. 2009a, Figure 19, right).

From value ε we can estimate the mass ratio of stellar components q: $q = M_{\rm RD}/M_{\rm WD}$. Kato (2022b) gave such an empirical dependence between q and ε^*, where $\varepsilon^* = \varepsilon/(1+\varepsilon)$: $q = 0.036(4) + 3.25\ (17)\ \varepsilon^*$ (see Figure 10), and from this equation the mass ratio $q = 0.099$.

Based on the correlation depicted in Figure 7 in Kato & Osaki (2013) it is possible to determine that for stage B at $\varepsilon = 0.020$, the mass ratio q is estimated to be 0.092. There is also a connection between the mass ratio q and the orbital period. Applying the relationship presented in Figure 1 in Kato (2022b), we obtain $q = 0.085 \pm 0.03$. And finally, using the relation q and $P_{\rm dot}$ according to the formula $q = 0.0043(9) P_{\rm dot} \cdot 10^{-5} + 0.060(5)$ (Equation (6) in Kato 2015), we find that $q = 0.095$. Therefore the average mass ratio q found by these four dependencies is equal to 0.09 ± 0.01.

According to Knigge et al. (2011) (Tables 2, 6, Figure 9), masses of red dwarfs in cataclysmic binary systems can be approximately estimated as $0.07 \pm 0.015\ M_{\rm Sun}$. Since we found the value $q = M_{\rm RD}/M_{\rm WD} = 0.09 \pm 0.01$ for ASASSN-19oc, the mass of the WD in this system will be equal to $M_{\rm WD} = 0.75 \pm 0.15\ M_{\rm Sun}$.

Note that the orbital period we found (80 minutes) is very close to the period limit for cataclysmic variables. Theoretical calculations give a minimum period of 65–80 minutes, and recently McAllister et al. (2019) from observations found this value to be 79 minutes.

This period limit is explained by the properties of the secondary component. As shown by Barker & Kolb (2003), Knigge et al. (2011), with such orbital period values, the secondary star is no longer able to maintain thermal equilibrium, as it cannot contract rapidly enough to the radius required for thermal equilibrium.

The mass of the secondary component in this case will be less than $0.07\ M_{\rm Sun}$, thermonuclear reactions at such masses stop and the star becomes a slowly evolving brown dwarf. Such systems are called "period bouncers" (Kolb & Baraffe 1999). Among the objects or candidates for these objects we can mention the studies of EG Cnc (Kimura et al. 2021), BW Scl (Neustroev & Mäntynen 2023), QZ Lib (Pala et al. 2018), and 15 stars from McAllister et al. (2019).

[11] http://argonaut.skymaps.info/
[12] https://stilism.obspm.fr/
[13] https://astro.acri-st.fr/gaia_dev/

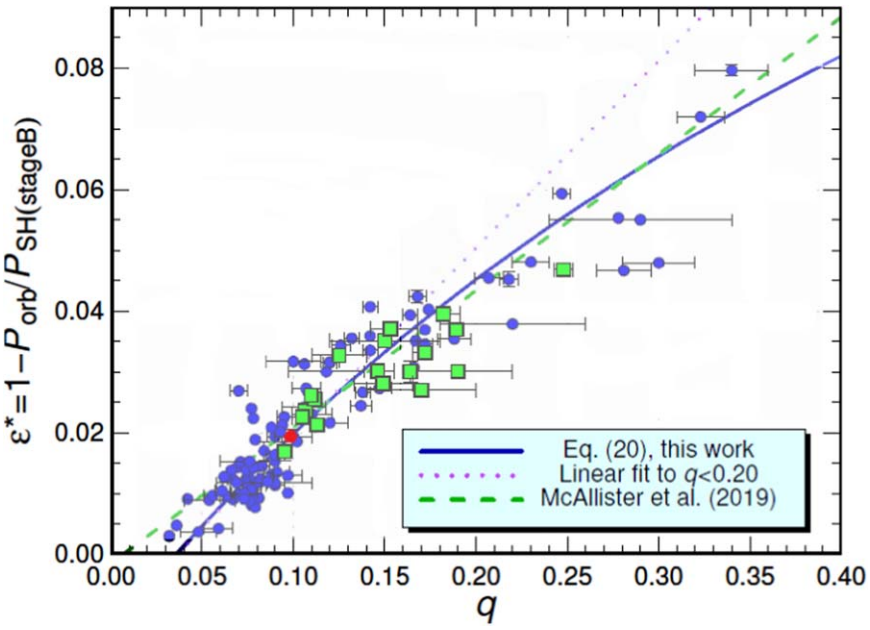

Figure 10. Dependence of q on ε^* (Figure 7 in Kato 2022b). The calculated value q for ASASSN-19oc is shown with a red circle.

Hence, the probability that there is a brown dwarf in our system is very high, and we draw the attention of researchers to this fact. For a more confident explanation of the physics of the processes occurring on the studied variable, it is necessary to obtain a radial velocity curve and calculate more accurate values of the masses of the components.

Upon knowing the masses and orbital period, we can estimate the distance a between the components in the system using Kepler's 3rd law, modified by Newton. Thus, $a = 0.57 \pm 0.03\, R_{\rm Sun}$.

Such values are in good agreement with the evolutionary tracks of cataclysmic variables (see Knigge et al. 2011, Tables 3–6).

3.4. Summary

We present optical observations of ASASSN-19oc during the superoutburst in 2019 June, as well as the outburst we detected on photographic plates from 1984. The following physical parameters were found:

1. intervals between outbursts are no more than ~35 yr,
2. period of early superhumps (which coincides with the orbital period), $P_{\rm ear} = 0.055685$ day, and based on this we suggested that the secondary component could be a brown dwarf candidate,
3. average period of ordinary superhumps, $P_{\rm ord} =$ 0.05681 (10) day,
4. rate of change of ordinary superhumps, $P_{\rm dot} = 8.1 \times 10^{-5}$,
5. the value of superhump excess, $\varepsilon = 0.020$.

We also rated:

1. average interstellar reddening, $E(B-V) = 0.12$ mag,
2. the color temperature T during a superoutburst, ~11,000 K,
3. mass ratio of binary's components, $q = 0.09$,
4. distance between components, $a \sim 0.57 \pm 0.03\, R_{\rm Sun}$
5. distance to the system d is about 560 ± 50 pc.

Based on the presence of early superhumps, characteristic values of the found parameters during the superoutburst, and the historical outburst that occurred in 1984, we confirm that ASASSN-19oc is a WZ Sge-type star with the superoutburst amplitude of about 7 mag. We also note that after the studied superoutburst, no rebrightenings were found in this object.

Acknowledgments

This research was carried out with the financial support of the APVV-20-0148, VEGA 2/0030/21 and VEGA 2/0031/22 grants, and the Scholarship of the Slovak Academic Information Agency SAIA. V.K. acknowledges the support from the Government Office of the Slovak Republic within EU NextGenerationEU through the Recovery and Resilience Plan for Slovakia under the project No. 09I03-03-V01-00002. We also thank the private company 4pi Systeme GmbH for partial sponsorship of this work. Also, we are very grateful to the anonymous reviewers for their valuable advice and comments on this work.

ORCID iDs

Viktoriia Krushevska https://orcid.org/0000-0002-6462-7107

References

Bailey, J. 1980, MNRAS, 190, 119
Barker, J., & Kolb, U. 2003, MNRAS, 340, 623
Bruch, A. 1984, A&AS, 56, 441
Buat-Ménard, V., & Hameury, J. M. 2002, A&A, 386, 891
Cannizzo, J. K., & Kenyon, S. J. 1987, ApJ, 320, 319
Capitanio, L., Lallement, R., Vergely, J. L., Elyajouri, M., & Monreal-Ibero, A. 2017, A&A, 606, A65
Deeming, T. J. 1975, Ap&SS, 36, 137
Echevarría, J. 1984, RMxAA, 9, 99
Echevarría, J., & Jones, D. 1983, RMxAA, 5, 301
Frohmaier, C., Swann, E., Short, P., et al. 2019, TNSAN, 27, 1
Gaia Collaboration, Brown, A. G. A., Vallenari, A., et al. 2021, A&A, 649, A1
Giovannelli, F. 2008, ChJAS, 8, 237
Green, G. M., Schlafly, E., Zucker, C., Speagle, J. S., & Finkbeiner, D. 2019, ApJ, 887, 93
Hameury, J.-M., Lasota, J.-P., & Warner, B. 2000, A&A, 353, 244
Han, Z., Boonrucksar, S., Qian, S., et al. 2020, PASJ, 72, 76
Harrop-Allin, M. K., & Warner, B. 1996, MNRAS, 279, 219
Harvey, D., Skillman, D. R., Patterson, J., & Ringwald, F. A. 1995, PASP, 107, 551
Hellier, C. 2001, Cataclysmic Variable Stars (Chichester: Springer-Praxis)
Hessman, F. V., Robinson, E. L., Nather, R. E., & Zhang, E. H. 1984, ApJ, 286, 747
Hirose, M., & Osaki, Y. 1990, PASJ, 42, 135
Hubeny, I., & Long, K. S. 2021, MNRAS, 503, 5534
Idan, I., Lasota, J. P., Hameury, J. M., & Shaviv, G. 2010, A&A, 519, A117
Imada, A., Kubota, K., Kato, T., et al. 2006, PASJ, 58, L23
Jacques, C., Barros, J., Pimentel, E., & Holvorcem, P. 2019, TNSTR, 2019-916, 1
Kato, T. 2015, PASJ, 67, 108
Kato, T. 2022a, arXiv:2205.05284
Kato, T. 2022b, arXiv:2201.02945
Kato, T., Imada, A., Uemura, M., et al. 2009a, PASJ, 61, S395
Kato, T., Ishioka, R., Isogai, K., et al. 2016a, PASJ, 68, 107
Kato, T., Isogai, K., Hambsch, F.-J., et al. 2017, PASJ, 69, 75
Kato, T., Nogami, D., Baba, H., & Matsumoto, K. 1998, in ASP Conf. Ser. 137, Wild Stars in the Old West, ed. S. Howell, E. Kuulkers, & C. Woodward (San Francisco, CA: ASP), 9
Kato, T., & Osaki, Y. 2013, PASJ, 65, 115
Kato, T., Pavlenko, E. P., Maehara, H., et al. 2009b, PASJ, 61, 601
Kato, T., Pavlenko, E. P., Shchurova, A. V., et al. 2016b, PASJ, 68, L4
Kimura, M., Isogai, K., Kato, T., et al. 2021, PASJ, 73, 1
Knigge, C., Baraffe, I., & Patterson, J. 2011, ApJS, 194, 28
Kolb, U., & Baraffe, I. 1999, MNRAS, 309, 1034
Kromer, M., Nagel, T., & Werner, K. 2007, A&A, 475, 301
Lallement, R., Babusiaux, C., Vergely, J. L., et al. 2019, A&A, 625, A135
Lallement, R., Vergely, J. L., Valette, B., et al. 2014, A&A, 561, A91
Landolt, A. U. 2009, AJ, 137, 4186
Lasota, J.-P. 2001, NewAR, 45, 449
Lasota, J.-P. 2023, arXiv:2311.16013
Lee, Y., Moon, D.-S., Kim, S. C., et al. 2019, ApJ, 880, 109
Lubow, S. H. 1991, ApJ, 381, 259
Mayo, S. K., Wickramasinghe, D. T., & Whelan, J. A. J. 1980, MNRAS, 193, 793
McAllister, M., Littlefair, S. P., Parsons, S. G., et al. 2019, MNRAS, 486, 5535
Meyer, F., & Meyer-Hofmeister, E. 2015, PASJ, 67, 52
Nakata, C., Ohshima, T., Kato, T., et al. 2013, PASJ, 65, 117
Namekata, K., Isogai, K., Kato, T., et al. 2017, PASJ, 69, 2
Neustroev, V. V., & Mäntynen, I. 2023, MNRAS, 523, 6114
Neustroev, V. V., Marsh, T. R., Zharikov, S. V., et al. 2017, MNRAS, 467, 597
Ohshima, T., Kato, T., Pavlenko, E., et al. 2014, PASJ, 66, 67
Osaki, Y. 1989, PASJ, 41, 1 005
Osaki, Y. 1996, PASP, 108, 39
Osaki, Y. 2005, PJAB, 81, 291
Osaki, Y., & Meyer, F. 2003, A&A, 401, 325
Pala, A. F., Schmidtobreick, L., Tappert, C., Gänsicke, B. T., & Mehner, A. 2018, MNRAS, 481, 2523
Ringwald, F. A., Velasco, K., Roveto, J. J., & Meyers, M. E. 2012, NewA, 17, 433
Shappee, B. J., Prieto, J. L., Grupe, D., et al. 2014, ApJ, 788, 48
Sion, E. M. 1999, PASP, 111, 532
Smak, J. 2000, NewAR, 44, 171
Smak, J. 2009, AcA, 59, 121
Smak, J. 2020, AcA, 70, 317
Soejima, Y., Imada, A., Nogami, D., Kato, T., & Monard, B. 2009, PASJ, 61, 395
Szegedi, H., Odendaal, A., Meintjes, P., et al. 2017, The Golden Age of Cataclysmic Variables and Related Objects IV (Palermo: PoS), 21
Szkody, P., Piche, F., & Feinswog, L. 1990, ApJS, 73, 441
Taguchi, K. 2023, ATel, 15857, 1
Tampo, Y., Isogai, K., Kojiguchi, N., et al. 2021, PASJ, 73, 753
Tampo, Y., Isogai, K., Kojiguchi, N., et al. 2022, PASJ, 74, 1287
Thomas, D. M., & Wood, M. A. 2015, ApJ, 803, 55
Udalski, A. 1988, AcA, 38, 315
Uemura, M., Mennickent, R. E., Ishioka, R., et al. 2005, A&A, 432, 261
Warner, B. 1995, Cataclysmic Variable Stars, Vol. 28 (Cambridge: Cambridge Univ. Press)
Whitehurst, R. 1988, MNRAS, 232, 35
Whitehurst, R., & King, A. R. 1989, in ESA Special Publication, Vol. 1, Two Topics in X-Ray Astronomy, Volume 1: X Ray Binaries. Volume 2: AGN and the X Ray Background, ed. J. Hunt & B. Battrick (The Netherlands: ESA Publications Division), 127
Wood, M. A., & Burke, C. J. 2007, ApJ, 661, 1042
Wood, M. A., Thomas, D. M., & Simpson, J. C. 2009, MNRAS, 398, 2110
Zorotovic, M., & Schreiber, M. R. 2020, AdSpR, 66, 1080